Resolving the step size in condensin-driven DNA loop extrusion identifies ATP binding as the step-generating process

Je-Kyung Ryu[1], Sang-Hyun Rah[1], Richard Janissen[1], Jacob W. J. Kerssemakers[1], and Cees Dekker[2,$]

Department of Bionanoscience, Kavli Institute of Nanoscience Delft, Delft University of Technology, Delft, Netherlands.

[1]These authors contributed equally to this work.

[2]Lead Contact

[$]Corresponding author: C.Dekker@tudelft.nl

SUMMARY

The condensin SMC protein complex organizes chromosomal structure by extruding loops of DNA. Its ATP-dependent motor mechanism remains unclear but likely involves steps associated with large conformational changes within the ~50 nm protein complex. Here, using magnetic tweezers, we resolve single steps in loop extrusion by individual yeast condensins. Step sizes range between 20-45 nm at forces of 1.0-0.2 pN, respectively, comparable to the complex size. The large steps show that condensin reels in DNA in very sizeable amounts, up to ~600 bp per extrusion step, consistent with the non-stretched DNA polymer at these low forces. Using ATP-binding-impaired and ATP-hydrolysis-deficient mutants, we find that ATP binding is the primary step-generating stage underlying DNA loop extrusion. We discuss the findings in terms of a scrunching model where a stepwise DNA loop extrusion is generated by an ATP-binding-induced engagement of the hinge and the globular domain of the SMC complex.

KEYWORDS: Condensin, magnetic tweezers, molecular motor, DNA loop extrusion, SMC proteins, step size

INTRODUCTION

Structural maintenance of chromosome (SMC) protein complexes, such as condensin, cohesin, and SMC5/6, are vital in many genetic processes, including mitotic chromosome organization and segregation, regulation of sister chromatid pairing, DNA damage repair and replication, and regulation of gene expression (Hirano, 2016; Jeppsson et al., 2014; Nasmyth and Haering, 2005; Rowley and Corces, 2018; Ruiten et al., 2018; Uhlmann, 2016). Emerging evidence points to SMC complexes as universal DNA-extrusion enzymes that play a key role in the macroscale chromosome organization. Chromosome-conformation-capture studies (Hi-C and variants;(Gibcus et al., 2018; Naumova et al., 2013) and 3D polymer simulations showed that loop extrusion by condensin can efficiently generate compaction of chromatin fibers (Alipour and Marko, 2012; Goloborodko et al., 2016). Recent *in vitro* single-molecule fluorescence imaging (Ganji et al., 2018; Golfier et al., 2020; Kim et al., 2020, 2019; Kong et al., 2020; Terakawa et al., 2017) demonstrated that SMC complexes extrude DNA into large loops by an ATP-dependent mechanochemical motor activity. These studies showed that the condensin complex constitutes a motor that reels in and extrudes DNA at a very high speed (~600 bp/s) while consuming only very low amounts of ATP (~2 ATP/s) (Ganji et al., 2018), implying that extrusion proceeds in large steps of the order of the ~50 nm condensin size. However, the underlying mechanism of DNA extrusion that leads to the generation of large DNA loops in a step-wise fashion remains to be elucidated.

Structural studies of condensin have suggested various sizeable conformational changes of the protein complex that are potentially associated with the loop-extrusion stepping (Hassler et al., 2018; Lee et al., 2020; Ryu et al., 2020; Yoshimura et al., 2002). Condensin consists of a ring formed by two 50 nm long antiparallel coiled-coil SMC arms that are mutually engaged by a hinge domain, and, at the opposite site of the ring, a globular domain consisting of two ATPase heads of the SMCs, the Brn1 kleisin, and two HEAT-repeat domains, Ycs4 and Ycg1 (Fig. S1). A recent AFM study (Ryu et al., 2020) showed large reversible hinge-to-globular domain motions of 22 ± 13 nm. Regarding the mechanochemical ATP hydrolysis cycle that drives the DNA extrusion, this recent AFM study of yeast condensin as well as a cryo-EM study of human cohesin demonstrated that ATP binding induces large conformational changes of the hinge domain (Higashi et al., 2020; Ryu et al., 2020; Shi et al., 2020). In attempts to measure condensin-mediated DNA extrusion step sizes, previous single-molecule magnetic tweezers (MT) studies showed significantly varying values, ranging from ~80 nm for *Xenopus* condensin I (Strick et al., 2004) to ~200 nm for yeast condensin (Eeftens et al., 2017) – significantly larger than the 50 nm condensin complex size that one intuitively would expect. The large reported step sizes are potentially affected by the intrinsically large

thermal motion of the DNA tethers, which renders it very challenging to perform high-resolution step-size measurements at the very low DNA stretching forces where condensin is active (< 1 pN; (Eeftens et al., 2017; Ganji et al., 2018). To elucidate the origin of the large discrepancies in previously reported step sizes, which bears direct relevance for the modelling of the loop-extrusion process, an accurate step size measurement of condensin-induced DNA loop extrusion is much needed.

In this study, we aimed to accurately measure single DNA-loop-extrusion step sizes as well as identify the step-generating process in the ATP mechanochemical cycle using high-throughput single-molecule magnetic tweezers (MT). We optimized the MT using a relatively short 1.5 kbp DNA construct to resolve small steps with a resolution down to ~10 nm even at the sub-picoNewton forces where condensin is active. We found that individual condensins do extrude loops of DNA in a step-wise fashion, with a force-dependent step size ranging from 17 ± 14 to 45 ± 38 nm (median ± SD) at 1.0 - 0.2 pN DNA stretching forces, respectively. Notably, these step sizes do not correspond to 50-135 base pair steps along DNA as one might assume, but involve the reeling in of DNA at much larger amounts of up to ~600 base pairs per step, consistent with the non-stretched behavior of the DNA polymer at these low forces. Importantly, the use of an ATP-binding-deficient Q-loop mutant and especially an ATP-hydrolysis-deficient EQ mutant unequivocally demonstrated that ATP binding is the primary step-generating process during DNA extrusion, while ATP hydrolysis enables the motor to perform subsequent DNA extrusion step cycles in a consecutive fashion.

RESULTS

Magnetic tweezers resolve single DNA extrusion steps of individual condensins

In order to resolve single DNA-loop-extrusion steps that are induced by an individual *S. cerevisiae* condensin holocomplex in real-time, we employed a single-molecule assay based on MT (De Vlaminck et al., 2011). MT are a particular advantageous technique because it allows to observe real-time DNA length changes at the single-molecule level at a high spatiotemporal resolution (~20 ms and ~2 nm, dependent on force) (Van Loenhout et al., 2012). Notably, at the very low < 1 pN DNA stretching forces where condensin is active, it is very challenging to perform high-resolution step-size measurements because of the intrinsically large Brownian motion of DNA-tethered magnetic beads. For this reason, we here optimized the MT technique by using a short DNA construct (1.5 kbp) to minimize the Brownian motion to its limits such that we could detect very small steps down to a resolution of ~10 nm even at sub-pN forces.

Furthermore, we measured up to 300 DNA tethers simultaneously with instrumental drift compensation at a frequency of 50 Hz, which provides large data sets suited for statistically robust analysis (Eeftens et al., 2017; Janissen et al., 2018, 2020).

More specifically, we tethered torsionally unconstrained, linear 1.5 kbp dsDNA molecules between magnetic beads and a glass surface (Fig. 1A). At a constant applied force of 8 pN, a very low concentration (1 nM) of condensin together with 1 mM ATP was injected to the flow cell, using the same buffer conditions that were previously used to study single condensin-mediated DNA loop extrusion (Ganji et al., 2018). After incubation for 8 minutes, the applied force was suddenly lowered to a force below 1 pN (0.2 pN in the example of Fig. 1B) to monitor the stepwise decrease in the DNA end-to-end length, which resulted from condensin-driven DNA loop extrusion activity (Fig. 1B; left), until the DNA was extruded to an extent that the magnetic bead reaches the surface after a few steps. Importantly, without ATP, changes in DNA lengths were never observed, confirming that the reduction in DNA lengths in presence of ATP resulted from an ATP-dependent DNA-loop-extrusion processes (Fig. 1B; right), in agreement with previous studies (Eeftens et al., 2017; Strick et al., 2004). Counting the fraction of DNA tethers that exhibited a stepwise reduction in apparent DNA length (Fig. 1C), we found that 60% of the tethers showed such loop extrusion activity at this low 1 nM concentration. The fact that 40% of the DNA tethers showed no activity indicates that the observed DNA extrusion is mediated by single condensin complexes, since, assuming a Poisson distribution for the number of active condensin complexes acting on a single DNA tether, the calculated average number λ of acting condensins per DNA molecule is $\lambda = 0.9$ (from $\lambda^0 e^{-\lambda}/0! = 0.4$), a number that is in good agreement to a previous single-molecule fluorescence-based DNA-loop-extrusion study conducted at comparable concentrations (Ganji *et al*., 2018).

Magnetic tweezers can be optimized to resolve 10-20 nm step sizes at sub-pN forces

We determined the minimally resolvable step size for different DNA tether lengths at forces ranging from 0.2-5 pN. The resolvable step size is largely limited by the intrinsic noise in MT measurements due to force-dependent bead fluctuations resulting from Brownian motion (Ostrofet *et al*., 2018). To quantitatively assess the resolution of our assay, we induced artificial steps of different sizes (ΔZ = 8.4, 16.8, 25.2, 33.6, 42.0 nm) by changing the focal plane relative to the DNA-tethered magnetic bead (Fig. 2A), and subsequently determining to what extent we could resolve these user-induced steps. The example traces shown in Figure 2B show that, as expected, the observable Brownian noise reduced at higher forces force. In order to relocate the induced steps (Fig. 2B: top), we applied a step-finding algorithm (Kerssemakers *et*

al., 2006) to fit our trace data using Chi-squared minimization without any fit parameter boundaries with respect to step sizes or locations. The example traces in Figure 2B show that at high force (5 pN) the smallest induced step size of ΔZ = 8.4 nm could readily be relocated, while at the lowest applied force (0.2 pN), the smallest steps drowned into the noise.

In order to determine the minimal detectable step size at different forces, we applied a validation algorithm that compared the detected steps by the step-finding algorithm with the artificially induced steps (Fig. 2C; red lines and blue lines, respectively). We defined a step relocation as 'successful', if both the step size and the dwell time were close to the user-induced values. The example traces shown in Figure 2C for 1.0 (top) and 0.2 pN (bottom) show the comparison for induced steps of ΔZ = 16.8 nm. Successful relocations are indicated with green triangles, whereas red triangles are false negatives, i.e., induced steps that remained undetected. Over a range of step sizes and forces, this validation procedure was repeated for ~100 traces with 40 induced steps at each condition. From the results shown in Figure 2D, we observed that lower forces led to a lower relocation success, as expected. Defining the step-detection limit as the step size where 50% (Fig. 2D: dotted line) of the induced steps were relocated successfully, we found that the step detection limit decreased from 16 to 6 nm for applied forces that increased from 0.3 pN to 5 pN, respectively.

Figure 2E displays the detection limit as a function of force for various DNA lengths. The obtained step detection limits closely followed the trend of the bead's Brownian noise in the z position over the entire tested force range (Figs. 2E, S2: dashed lines). This indicates that Brownian noise is the dominant parameter that determines the step detection limit. Longer DNA tethers with lengths of 3.4 and 10 kbp exhibited higher step detection limits than the 1.5 kbp DNA tethers. The assay with the 1.5 kbp DNA construct provided step detection limits below 20 nm, ranging from ~6 to ~20 nm, throughout the entire 0.2-5.0 pN force range tested. Importantly, these low detection limits are well below the ~50 nm size of the condensin complex and thus below the putative step size in loop extrusion. In all subsequent DNA-loop-extrusion experiments, we used the 1.5 kbp DNA construct for measuring step sizes.

Condensin-induced DNA loop extrusion exhibits a broad distribution of step sizes

Now well set up to resolve small steps, we characterized the steps in DNA loop extrusion induced by condensin under various conditions. Figure 3A shows a typical data trace, where two distinct signatures are observed: a series of consecutive downward steps (Fig. 3A; left inset), which was the generic DNA loop-extrusion behavior, as well as occasionally a downward step that was followed by a single reverse step

upwards (Fig. 3A; right inset). Such reverse upward steps occurred exclusively after a prior downward step. Employing our step-detection algorithm to the experimental data at 0.4 pN, we identified the distribution of step sizes, as can be seen in Figure. 3B.

Notably, the step size distribution was found to be very broad, covering a wide range of small and large step sizes. The median step size was found to be comparable for downward and reverse steps, i.e., 32 ± 26 nm for downward steps versus 31 ± 29 nm for reverse steps (both median ± SD). In the absence of ATP, no step signatures were observed (Fig. 3C). The measured dwell times (Fig. S3A) followed a single exponential distribution for both downward and upward steps, suggesting that the steps originated from a simple one-rate-limiting process. Individual DNA extrusion steps almost exclusively were very fast, i.e., occurring within a single 20 ms imaging frame.

The key result of Figure 3B is the observed median step size value of 32 nm, which is twice higher than the step detection limit of 17 nm (Figs. 2E, S3B) at this 0.4 pN force. To further validate our result, we compared the experimental data with the step sizes deduced for the user-induced 33.6 nm steps (Fig. S3C), which are close in value to the 32 nm median value in the condensin experiments. For this user-set step size, our validation test resulted in only a small spread of ~15 nm (SD), indicating that tracking and step-finding analysis errors were not causing the broad distribution observed for the condensin stepping.

Condensin extrudes DNA in steps of tens of nm, reeling in DNA up to 600 bps per step

We observed a pronounced force dependence of the stepping behavior which reduced with increasing force (Fig. 3E, F). Above 1 pN, we could not observe any significant loop extrusion activity, in agreement with previous observations (Eeftens et al., 2017; Ganji et al., 2018). Figure 3F show the distribution of observed step size from 0.2 pN to 1 pN, which exhibited a distinctly narrower distribution at higher forces. The ratio between reverse and downward steps was largely maintained at a value of about 0.3 at all tested forces (Fig. S3D, E).

A major result of this work is displayed in Figure 3G and H, which plot the median step size versus applied force. Step size values ranged from 17 ± 14 to 45 ± 38 nm (median ± SD) between 1 and 0.2 pN, respectively. The measured values were at all forces significantly larger than the step detection limits (grey lines). The width of the step size distributions decreased from 38 nm (SD at 0.2 pN) to 14 nm (SD at 1.0 pN) upon application of higher force (Fig. S3D, F). Upon conversion of the measured step sizes in nm to force-dependent DNA steps measured in bp, using a prior measured standard relationship between DNA end-to-end length and force (Fig. S4), we found that the steps of extruded length of DNA also exhibited a

notable force dependence, yielding steps from 100 bp up to 600 bp between 1 and 0.2 pN (Fig. 3H), respectively. This force dependence as well as the large value of 600 bp (which clearly exceeds the ~150 bp that would be expected if a step would correspond to reeling in 50 nm of straight DNA) suggest that in each step, loop extrusion proceeds by grabbing DNA from somewhere within the random polymer blob that DNA forms due to its nature as a non-stretched semiflexible polymer at these low forces.

ATP binding is the step-generating stage in the ATP hydrolysis cycle that underlies condensin-mediated DNA loop extrusion

While it is established that condensin extrudes DNA loops in an ATP-hydrolysis-dependent manner (Eeftens et al., 2017; Ganji et al., 2018), our MT experiments interestingly allow to discriminate between the mechanochemical functions of ATP binding and ATP hydrolysis through the study of ATP-mutants of condensin. Specifically, we studied the DNA extrusion stepping behavior of the EQ mutant ($Smc2_{E1113Q}$-$Smc4_{E1352Q}$) which allows ATP binding but blocks its hydrolysis by a Walker B mutation in the ATPase domains, as well as for the Q-loop mutant ($Smc2_{Q147L}$-$Smc4_{Q302L}$), which blocks ATP binding to the ATPase domain entirely. Contrary to the wild-type condensin (Fig. 4A), the EQ mutant was not able to perform consecutive DNA extrusion steps. Instead, the EQ mutant was solely capable of performing single downward steps (Fig. 4B), which sometimes was followed by a reverse step (Fig. 4C). The Q-loop mutant did not show any step activity (Fig. 4D). The relative occurrence of the different step signatures of observed activity (i.e. consecutive downward steps, single downward steps, single downward followed by reverse step pairs, and inactive traces) is shown in Figure 4E. The data clearly demonstrates the necessity of ATP hydrolysis to perform consecutive DNA extrusion steps, while ATP binding (without subsequent hydrolysis) only allows to perform single steps.

The distribution of step sizes as well as the force dependence of the step size for the EQ mutant (Fig. 4F-H) was very similar to the WT condensin. The results indicate that the ATP-binding-dependent step for the EQ mutant is identical to the WT step formation, and establish that ATP binding is the primary step-generating process within the ATP hydrolysis cycle.

DISCUSSION

Using MT with short 1.5 kbp DNA tethers that allow the detection of DNA loop extrusion steps as small as 10-20 nm in the relevant low-force regime, we resolved that condensin extrudes DNA in a stepwise

fashion, with a median step size of the order of 20-45 nm at DNA stretching forces from 1 to 0.2 pN, respectively. Furthermore, we identified that ATP binding is the primary step-generating process during DNA loop extrusion. Below, we discuss several of the most salient findings.

Step sizes indicate large conformational changes of condensin during loop extrusion

The measured median step sizes ranged between 20 and 45 nm over the relevant range of forces where condensin is active, which amounts to a good fraction of the longest dimension of the condensin holocomplex as the length of the SMC coiled coils is about 50 nm. The observed very large step sizes define SMCs as an entirely distinct class of DNA-processing motor proteins that are unlike any other DNA-processing enzymes reported before (e.g. helicase, translocases, polymerases), which translocate in single-base pair steps upon each ATP hydrolysis cycle (Graham et al., 2010; Hsieh et al., 2015; Liu et al., 2014; Pease et al., 2005; Seidel et al., 2004; Sirinakis et al., 2011).

Our accurate measurements of the DNA-extrusion step size yielded a smaller value than previous estimates of ~80 nm (at 0.4 pN and 2 nM condensin, measured with 4 kbp DNA; (Strick et al., 2004) and ~200 nm (0.75 pN, 8.6 nM condensin, 20 kbp DNA; (Eeftens et al., 2017). As the noise increases with the DNA tether length (Fig. 2E), small DNA loop extrusion steps may have been overshadowed in these studies. In addition, higher condensin concentrations can readily increase the propensity of multiple condensins acting on a single DNA tether. Considering that the distribution of single condensin-mediated step sizes is very broad (Fig. 3B, D), noise in the earlier studies may have effectively cut off the smaller step sizes, yielding an average step size that exceeds the intrinsic value. Our observed range of average step sizes (20-45 nm), is, however, in good agreement with the recently reported hinge-to-globular domain distance of 22 ± 13 nm that is involved in a dynamic toggling between O to B shapes (Fig. S1) (Ryu et al., 2020). The large DNA step sizes also match quite well with values that can be guessed from combining the loop extrusion and ATPase rates in previous *in vitro* studies on condensin and cohesin with ~1 kbp/s and 2 ATP/s (Davidson et al., 2019; Ganji et al., 2018; Kim et al., 2019), and of SMC-ScpAB from *B. Subtilis* with ~800 bp/s and 1 ATP/s (Wang et al., 2017, 2018).

Large extrusion steps are associated with the structural flexibility of DNA at low forces

A broad distribution of condensin-mediated DNA loop extrusion step sizes was observed (Fig. 3B, F), with a variation in step sizes that was well beyond that set by the instrumentation, as can be seen from the

much more narrow variation in the user-induced step sizes in our step-validation tests (Figs. 3D, S3B,C). One contribution to the variation in measured DNA extrusion step sizes could be a variation in the degree of internal conformational changes of the condensin, similar to a sizeable variation (SD = 13 nm) in the hinge-to-head motion that was observed in AFM (Ryu et al., 2020). Much more importantly, however, is the variation that is induced by the structurally very flexible and dynamic nature of DNA at these very low stretching forces. Infrequently, and particularly at the lowest force, we observed very large step sizes of ~100 nm, which clearly exceeded the ~50 nm size of the condensin complex. We envision that such steps result from a condensin complex that 'grabs' DNA from a relatively remote location during a temporal excursion.

Indeed, our observation that step sizes can correspond up to an amount of 600 bp per step supports the notion that condensin is able to bind to a remote region of DNA within the polymer blob of non-stretched, flexible, and dynamic DNA, to subsequently reel it in. Accordingly, the observed strong force-dependence of the step size can be attributed to the polymeric nature of the DNA, with smaller steps at higher forces when the DNA is increasingly stretched out. The fact that DNA extrusion step sizes are dependent on the force due to the polymeric nature of DNA, is entirely different from the characteristics of motor proteins such as myosin and kinesin (Carter and Cross, 2005; Clemen et al., 2005; Mehta A.D. et al., 1999), which walk along stiff protein filaments (Gittes et al., 1993). We found that the mechanical work ($Force \times Stepsize$) done during a single DNA extrusion step slightly increased with force (Fig. S3G). If we assume that the stepping is associated with a cycle that involves the hydrolysis of a single ATP (i.e., an energy of 20 k_BT), the energy efficiency would range from 12 to 20 % for forces from 0.2 to 1.0 pN, respectively, a number that is not uncommon for other ATP-driven molecular motors (Lee and Yang, 2006; Thomsen and Berger, 2009). Furthermore, the found stall force of ~1 pN for DNA loop extrusion by condensin is very low compared to stall forces of other DNA-translocating motors, but in agreement with previous findings (Eeftens et al., 2017; Ganji et al., 2018).

ATP binding and hydrolysis relate to two distinct mechanistic processes

Our results unequivocally demonstrate that ATP *binding* is the process that is associated with the DNA-extrusion stepping, since the ATP hydrolysis-deficient EQ mutant (Fig. 4E) was able to make single steps, but unable to perform consecutive DNA extrusion steps, while the ATP-binding-deficient Q-loop mutant did not show any DNA extrusion activity. Consequently, and different from most other ATPase motor

proteins, ATP hydrolysis occurs downstream in the hydrolysis cycle to enable DNA extrusion steps in a consecutive manner.

Our finding that ATP binding is the step-generation process differs from a previously suggested DNA pumping model (Marko et al., 2019) that attributed ATP hydrolysis to the generation of a step, associated with the zipping-up of the SMC arms from an ATP-bound O shape into an ATP-unbound I shape that pushes DNA from the hinge to the head domains. By contrast, our result that ATP binding is the step-generating process is in good agreement with cryo-EM results on cohesin (Collier et al., 2020; Dao et al., 2018; Higashi et al., 2020; Shi et al., 2020) and with recent AFM data on condensin that showed a transition from an extended O shape to a collapsed B shape upon ATP binding (Ryu et al., 2020).

Our data are also in good agreement with a DNA scrunching model that we recently hypothesized based on these AFM data (Ryu et al., 2020), where condensin first anchors itself to DNA using the safety belt of the Ycg1-Brn1 domains (Fig. 4I i) (Ganji et al., 2018; Kschonsak et al., 2017), whereupon the hinge domain binds to a proximate region of the DNA, and ATP binding induces a transition from an extended O shape to a collapsed B shape, thereby pulling the hinge-bound DNA to the globular domain (Fig. 4I ii), which establishes a step in the loop extrusion process. In support of this concept, previous studies showed that ATP binding induces the dimerization of the head domains, forming a positively charged cavity that is able to bind DNA (Erickson, 2009; Hassler et al., 2019; Liu et al., 2016; Seifert et al., 2016; Shi et al., 2020; Woo et al., 2009). The low stalling force that we observed is consistent with a type of a motor mechanism that involves a Brownian ratchet motion of the flexible SMC arms that underlies the hinge to globular domain step. In the next stage of the cycle, ATP hydrolysis occurs whereupon the hinge is released and the condensin returns to the O shape where it is available to bind to a new DNA target site for the next step (Fig. 4I iii), thus closing the DNA loop extrusion cycle. Additional support for this scenario is provided by a prior study that showed that ATP hydrolysis induces the dissociation of the head dimers, hence disrupting the capability to bind DNA (Hassler et al., 2019). The model indicates that condensin may employ 'credit-card energetics' (Kowalczykowski, 2008) in which ATP binding induces a single step whereas the energy released upon ATP hydrolysis is coupled to downstream processes in the DNA loop extrusion, well after the step-generation upon ATP binding.

CONCLUSION

In conclusion, our experimental results demonstrate that the SMC proteins are unique protein complexes that can extrude DNA loops with very large step sizes up to 600 bp. Our study shows that DNA loop

extrusion steps consist of two distinct processes: ATP binding provides the step-generating process where likely DNA bound to the hinge domains is pulled to the globular domains, leading to DNA loop extrusion. In the second subsequent step, ATP hydrolysis presumably enables the hinge domain to target a next DNA site for a subsequent loop extrusion step. The observed strong dependence of step size on the applied DNA stretching force revealed that the flexible nature of the DNA polymer at very low stretching forces facilitates the extrusion of very large amounts of DNA in each step in the loop extrusion process. Our work reveals unique characteristics of the motor action of condensin which may be conserved among other SMC proteins that exhibit DNA loop extrusion.

SUPPLEMENTAL INFORMATION

Supplemental Information includes 4 figures, 1 table, and a detailed methodological description, and can be found online at https://doi.org/10.1016/j.molcel.xxxx.xx.xxx.

ACKNOWLEDGMENTS

We thank J. van der Torre for DNA construct synthesis, E. van der Sluis for protein purification, and R. Barth, A. J. Katan, E. Kim, B. Pradhan for discussions. We acknowledge Christian Haering for providing the condensin mutants. This work was supported by ERC grant LoopingDNA (883684) (to C.D.), Marie Sklodowska-Curie grant agreement No 753002. (to J.-K.R.), and the Netherlands Organization for Scientific Research (NWO/OCW) as part of the Frontiers of Nanoscience and Basyc programs.

AUTHOR CONTRIBUTIONS

C.D., J.-K.R. and J.W.J.K. conceived the project. All authors designed the experiments. J.W.J.K. and R.J. built the magnetic tweezers instrument. S.-H.R., R.J., J.W.J.K., and J.-K.R. performed magnetic tweezers experiments. J.W.J.K. and S.-H.R. constructed Matlab codes for a step-analysis, and S.-H.R, J.W.J.K.., J.-K.R., and R.J. performed analysis. All authors contributed to writing of the manuscript.

DECLARATION OF INTERESTS

The authors declare no competing interests.

REFERENCES

Alipour, E., and Marko, J.F. (2012). Self-organization of domain structures by DNA-loop-extruding enzymes. Nucleic Acids Res. *40*, 11202–11212.

Carter, N.J., and Cross, R.A. (2005). Mechanics of the kinesin step. Nature *435*, 308–312.

Clemen, A.E.M., Vilfan, M., Jaud, J., Zhang, J., Bärmann, M., and Rief, M. (2005). Force-dependent stepping kinetics of myosin-V. Biophys. J. *88*, 4402–4410.

Cnossen, J.P., Dulin, D., and Dekker, N.H. (2014). An optimized software framework for real-time, high-throughput tracking of spherical beads. Rev. Sci. Instrum. *85*, 103712.

Collier, J.E., Lee, B.G., Roig, M.B., Yatskevich, S., Petela, N.J., Metson, J., Voulgaris, M., Gonzalez Llamazares, A., Löwe, J., and Nasmyth, K.A. (2020). Transport of DNA within cohesin involves clamping on top of engaged heads by Scc2 and entrapment within the ring by Scc3. Elife *9*, 1–36.

Dao, T.P., Kolaitis, R.M., Kim, H.J., O'Donovan, K., Martyniak, B., Colicino, E., Hehnly, H., Taylor, J.P., and Castañeda, C.A. (2018). Ubiquitin Modulates Liquid-Liquid Phase Separation of UBQLN2 via Disruption of Multivalent Interactions. Mol. Cell *69*, 965-978.e6.

Davidson, I.F., Davidson, I.F., Bauer, B., Goetz, D., Tang, W., Wutz, G., and Peters, J. (2019). DNA loop extrusion by human cohesin. Science. *3418*, 1338–1345.

Eeftens, J.M., Bisht, S., Kerssemakers, J., Kschonsak, M., Haering, C.H., and Dekker, C. (2017). Real-time detection of condensin-driven DNA compaction reveals a multistep binding mechanism. EMBO J. *36*, e201797596.

Erickson, H.P. (2009). Size and shape of protein molecules at the nanometer level determined by sedimentation, gel filtration, and electron microscopy. Biol. Proced. Online *11*, 32–51.

Ganji, M., Shaltiel, I.A., Bisht, S., Kim, E., Kalichava, A., Haering, C.H., and Dekker, C. (2018). Real-time imaging of DNA loop extrusion by condensin. Science . *360*, 102–105.

Gibcus, J.H., Samejima, K., Goloborodko, A., Samejima, I., Naumova, N., Nuebler, J., Kanemaki, M.T., Xie, L., Paulson, J.R., Earnshaw, W.C., et al. (2018). A pathway for mitotic chromosome formation. Science . *359*.

Gittes, F., Mickey, B., Nettleton, J., and Howard, J. (1993). Flexural rigidity of microtubules and actin filaments measured from thermal fluctuations in shape. J. Cell Biol. *120*, 923–934.

Golfier, S., Quail, T., Kimura, H., Brugues, J., and Stefan Golfier, Thomas Quail, Hiroshi Kimura, J.B. (2020). Cohesin and condensin extrude DNA loops in a cell-cycle dependent manner. Elife 821306.

Goloborodko, A., Imakaev, M. V, Marko, J.F., and Mirny, L. (2016). Compaction and segregation of sister chromatids via active loop extrusion. Elife *5*, 1–16.

Hassler, M., Shaltiel, I.A., and Haering, C.H. (2018). Towards a Unified Model of SMC Complex Function. Curr. Biol. *28*, R1266–R1281.

Hassler, M., Shaltiel, I.A., Kschonsak, M., Simon, B., Merkel, F., Thärichen, L., Bailey, H.J., Macošek, J., Bravo, S., Metz, J., et al. (2019). Structural Basis of an Asymmetric Condensin ATPase Cycle. Mol. Cell 1175–1188.

Higashi, T.L., Eickhoff, P., Sousa, J.S., Locke, J., Nans, A., Flynn, H.R., Snijders, A.P., Papageorgiou, G., O'Reilly, N., Chen, Z.A., et al. (2020). A Structure-Based Mechanism for DNA Entry into the Cohesin Ring. Mol. Cell *79*, 917-933.e9.

Hirano, T. (2016). Condensin-Based Chromosome Organization from Bacteria to Vertebrates. Cell *164*, 847–857.

Janissen, R., Arens, M.M.A., Vtyurina, N.N., Rivai, Z., Sunday, N.D., Eslami-Mossallam, B., Gritsenko, A.A., Laan, L., de Ridder, D., Artsimovitch, I., et al. (2018). Global DNA Compaction in Stationary-Phase Bacteria Does Not Affect Transcription. Cell *174*, 1188-1199.e14.

Janissen, R., Eslami-Mossallam, B., Artsimovitch, I., Depken, M., and Dekker, N.H. (2020). A Unifying Mechanistic Model of

Bacterial Transcription with Three Interconnected Pause States and Non-Diffusive Backtrack Recovery. Biophys. J. *118*, 543a.

Jeppsson, K., Kanno, T., Shirahige, K., and Sjögren, C. (2014). The maintenance of chromosome structure: Positioning and functioning of SMC complexes. Nat. Rev. Mol. Cell Biol. *15*, 601–614.

Kerssemakers, J.W.J., Laura Munteanu, E., Laan, L., Noetzel, T.L., Janson, M.E., and Dogterom, M. (2006). Assembly dynamics of microtubules at molecular resolution. Nature *442*, 709–712.

Kim, E., Kerssemakers, J., Shaltiel, I.A., Haering, C.H., and Dekker, C. (2020). DNA-loop extruding condensin complexes can traverse one another. Nature *579*.

Kim, Y., Shi, Z., Zhang, H., Finkelstein, I.J., and Yu, H. (2019). Human cohesin compacts DNA by loop extrusion. Science. *366*, 1345–1349.

Klaue, D., and Seidel, R. (2009). Torsional stiffness of single superparamagnetic microspheres in an external magnetic field. Phys. Rev. Lett. *102*, 1–4.

Kong, M., Cutts, E.E., Pan, D., Beuron, F., Kaliyappan, T., Xue, C., Morris, E.P., Musacchio, A., Vannini, A., and Greene, E.C. (2020). Human Condensin I and II Drive Extensive ATP-Dependent Compaction of Nucleosome-Bound DNA. Mol. Cell *79*, 99-114.e9.

Kowalczykowski, S.C. (2008). Structural biology: Snapshots of DNA repair. Nature *453*, 463–466.

Kschonsak, M., Merkel, F., Bisht, S., Metz, J., Rybin, V., Hassler, M., and Haering, C.H. (2017). Structural Basis for a Safety-Belt Mechanism That Anchors Condensin to Chromosomes. Cell *171*, 588–600.

Lee, J.Y., and Yang, W. (2006). UvrD Helicase Unwinds DNA One Base Pair at a Time by a Two-Part Power Stroke. Cell *127*, 1349–1360.

Lee, B.G., Merkel, F., Allegretti, M., Hassler, M., Cawood, C., Lecomte, L., O'Reilly, F.J., Sinn, L.R., Gutierrez-Escribano, P., Kschonsak, M., et al. (2020). Cryo-EM structures of holo condensin reveal a subunit flip-flop mechanism. Nat. Struct. Mol. Biol.

Liu, Y., Sung, S., Kim, Y., Li, F., Gwon, G., Jo, A., Kim, A., Kim, T., Song, O., Lee, S.E., et al. (2016). ATP -dependent DNA binding, unwinding, and resection by the Mre11/Rad50 complex . EMBO J. *35*, 743–758.

Van Loenhout, M.T.J., Kerssemakers, J.W.J., De Vlaminck, I., and Dekker, C. (2012). Non-bias-limited tracking of spherical particles, enabling nanometer resolution at low magnification. Biophys. J. *102*, 2362–2371.

Marko, J.F., De Los Rios, P., Barducci, A., and Gruber, S. (2019). DNA-segment-capture model for loop extrusion by structural maintenance of chromosome (SMC) protein complexes. Nucleic Acids Res. *47*, 6956–6972.

Mehta A.D., Rock R.S., Rief M., Spudich J.A., Mooseker M.S., and Cheney R.E. (1999). Myosin-V is aprocessive actin-based motort. Nature *400*, 590–593.

Nasmyth, K., and Haering, C.H. (2005). the Structure and Function of Smc and Kleisin Complexes. Annu. Rev. Biochem. *74*, 595–648.

Naumova, N., Imakaev, M., Fudenberg, G., Zhan, Y., Lajoie, B.R., Mirny, L. a., and Dekker, J. (2013). Organization of the Mitotic Chromosome. Science . *342*, 948–953.

Ostrofet, E., Papini, F.S., and Dulin, D. (2018). Correction-free force calibration for magnetic tweezers experiments. Sci. Rep. *8*, 2–11.

Rowley, M.J., and Corces, V.G. (2018). Organizational principles of 3D genome architecture. Nat. Rev. Genet. *19*, 1.

Ruiten, M.S. Van, Rowland, B.D., van Ruiten, M.S., Rowland, B.D., Ruiten, M.S. Van, and Rowland, B.D. (2018). SMC Complexes: Universal DNA Looping Machines with Distinct Regulators. Trends Genet. *34*, 477–487.

Ryu, J., Katan, A.J., Sluis, E.O. Van Der, Wisse, T., Groot, R. De, Haering, C.H., and Dekker, C. (2020). The condensin holocomplex cycles dynamically between open and collapsed states. Nat. Struct. Mol. Biol.

Seifert, F.U., Lammens, K., Stoehr, G., Kessler, B., and Hopfner, K. (2016). Structural mechanism of ATP -dependent DNA binding and DNA end bridging by eukaryotic Rad50 . EMBO J. *35*, 759–772.

Shi, Z., Shi, Z., Gao, H., Bai, X., and Yu, H. (2020). Cryo-EM structure of the human cohesin-NIPBL-DNA complex. Science . *368*, 1–13.

Strick, T.R., Kowaguchi, T., and Hirano, T. (2004). Real-Time Detection of Single-Molecule DNA Compaction by Condensin I. Curr. Biol. *14*, 874–880.

Terakawa, T., Bisht, S., Eeftens, J.M., Dekker, C., Haering, C.H., and Greene, E.C. (2017). The condensin complex is a mechanochemical motor that translocates along DNA. Science. *358*, 672–676.

Thomsen, N.D., and Berger, J.M. (2009). Running in Reverse: The Structural Basis for Translocation Polarity in Hexameric Helicases. Cell *139*, 523–534.

Uhlmann, F. (2016). SMC complexes: From DNA to chromosomes. Nat. Rev. Mol. Cell Biol. *17*, 399–412.

De Vlaminck, I., Henighan, T., Van Loenhout, M.T.J., Pfeiffer, I., Huijts, J., Kerssemakers, J.W.J., Katan, A.J., Van Langen-Suurling, A., Van Der Drift, E., Wyman, C., et al. (2011). Highly parallel magnetic tweezers by targeted DNA tethering. Nano Lett. *11*, 5489–5493.

De Vlaminck, I., van Loenhout, M.T.J., Zweifel, L., den Blanken, J., Hooning, K., Hage, S., Kerssemakers, J., and Dekker, C. (2012). Mechanism of Homology Recognition in DNA Recombination from Dual-Molecule Experiments. Mol. Cell *46*, 616–624.

Wang, X., Brandão, H.B., Le, T.B.K., Laub, M.T., and Rudner, D.Z. (2017). Travel From Origin To Terminus. Science . *527*, 524–527.

Wang, X., Hughes, A.C., Brandão, H.B., Walker, B., Lierz, C., Cochran, J.C., Oakley, M.G., Kruse, A.C., and Rudner, D.Z. (2018). In Vivo Evidence for ATPase-Dependent DNA Translocation by the Bacillus subtilis SMC Condensin Complex. Mol. Cell *71*, 841-847.e5.

Woo, J.S., Lim, J.H., Shin, H.C., Suh, M.K., Ku, B., Lee, K.H., Joo, K., Robinson, H., Lee, J., Park, S.Y., et al. (2009). Structural Studies of a Bacterial Condensin Complex Reveal ATP-Dependent Disruption of Intersubunit Interactions. Cell *136*, 85–96.

Yoshimura, S.H., Hizume, K., Murakami, A., Sutani, T., Takeyasu, K., and Yanagida, M. (2002). Condensin Architecture and Interaction with DNA. Curr. Biol. *12*, 508–513.

STAR★METHODS

KEY RESOURCES TABLE

REAGENT or RESOURCE	SOURCE	IDENTIFIER
Antibodies		
Anti-Digoxigenin	Roche	Cat# 11333089001
Chemicals, Peptides, and Recombinant Proteins		
Biotin-16-dUTP	Jena Bioscience	Cat# NU-803-BIO16
Digoxigenin-11-dUTP	Jena Bioscience	Cat# NU-803-DIGX
ATP	Thermo Scientific	Cat# R0441
Bovine Serum Albumin	New England Biolabs	Cat# B9000S
BsaI-HFv2 restriction enzyme	New England Biolabs	Cat# R3733S
Polybead Microspheres 1.50 µm	Polysciences	Cat# 17133
Dynabeads MyOne Streptavidin	Thermo Scientific	Cat# 65601
Oligonucleotides		
Primers for Magnetic Tweezers DNA constructs	This work	See Table S1
Condensin proteins		
Wild-type condensin	(Eeftens et al., 2017)	N/A
EQ mutant condensin	(Eeftens et al., 2017)	N/A
Q-loop mutant condensin	(Eeftens et al., 2017)	N/A
Software and Algorithms		
MATLAB R2020a	MathWorks Inc.	www.mathworks.com
Igor Pro 6.37	Wavemetrics	www.wavemetrics.com
LabView 2011	National Instruments	www.ni.com

RESOURCE AVAILABILITY

Lead contact

Further information and requests for resources and reagents should be directed to and will be fulfilled by the Lead Contact (C.Dekker@tudelft.nl).

Materials availability

This study did not generate new unique reagents.

Data and code availability

All data and code are available upon requests.

METHOD DETAILS

Preparation of protein and DNA

S. cerevisiae wild type condensin, as well as the EQ ($Smc2_{E1113Q}$-$Smc4_{E1352Q}$) and Q-loop ($Smc2_{Q147L}$-$Smc4_{Q302L}$) mutants, were expressed and purified as previously described (Ganji et al., 2018).

Singly biotinylated linear dsDNA constructs with a length of 1.5, 3.4, and 10 kbp were synthesized *via* PCR and enzymatically ligated to digoxigenin-enriched DNA handles. Primers (Table S1) were obtained from Ella Biotech GmbH, Germany or Integrated DNA Technologies, Europe. Biotinylated DNA fragments of different length were produced by using biotin-labeled forward primers (1.5 kb: JT-273; 3.4 kb: TL-34; 10 kb: TL-101) and reverse primers (1.5 kb: JT-275; 3.4 kb: TL-35; 10 kb: TL-102) that contain a *Bsa*I restriction site (Table S1) on pBluescript II SK+. To create the digoxigenin (DIG)-enriched handles, a 485 bp fragment from pBluescript II SK+ (Stratagene, Agilent Technologies Inc., USA) was amplified by PCR in the presence of 1:5 Digoxigenin-11-dUTP:dTTP (Jena Bioscience, Germany) using primers CD21 and CD26 (Table S1). Prior to ligations of the DNA fragments and handles, all amplicons were digested with the non-palindromic restriction enzyme *Bsa*I-HFv2 (New England Biolabs, UK). The ligation of the DIG-handles and biotinylated DNA fragments was carried out overnight using T4 DNA ligase (New England Biolabs, UK).

Magnetic tweezers

The magnetic tweezers setup used in this study was as described previously (Janissen *et al*., 2018). Briefly, a pair of vertically aligned permanent neodymium-iron-boron magnets (Webcraft GmbH, Germany) 1 mm apart was used to generate the magnetic field. They were placed on a motorized stage (#M-126.PD2, Physik Instrumente) above the flow cell and allowed red LED light to pass through and illuminate the sample. The transmitted light was collected with a 50x oil-immersion objective (CFI Plan 50XH, Achromat; 50x; NA = 0.9, Nikon), and the bead diffraction patterns were recorded with a 4 megapixel CMOS camera (#Falcon 4M60; Teledyne Dalsa) at 50 Hz. If bead rotation was needed, the magnet pair was rotated with a DC servo step motor (C-150.PD; Physik Instrumente) around the illumination axis. Image processing of the bead diffraction patterns allowed us to track the real-time positions of DNA-bound magnetic beads and surface-bound polystyrene reference beads. The bead *x*, *y*, *z* position tracking was achieved using a cross-correlation algorithm in a custom LabView software (2011, National Instruments Corporation) (Cnossen et al., 2014; De Vlaminck et al., 2012). The software also applied spectral corrections to correct for camera blur and aliasing. Up to 300 beads were tracked simultaneously with an approximate Z-tracking resolution of ~2 nm.

Single-molecule condensin-driven loop-extrusion MT assay

Liquid flow cell preparation and DNA tethering has been described in detail elsewhere (Janissen et al., 2018). Briefly, streptavidin-coated superparamagnetic beads (MyOne DynaBeads, LifeTechnologies, USA) with a diameter of 1 µm were used within this study. Commercially available polystyrene beads (Polysciences GmbH, Germany) with a diameter of 1.5 µm were used as reference beads fixed to the glass surfaces. The polystyrene reference beads were diluted 1:1500 in PBS buffer (pH 7.4; Sigma Aldrich) and then adhered to the KOH-treated (Invitrogen) flow cell glass surface. Afterwards, digoxigenin antibodies (Roche Diagnostics) at a concentration of 0.1 mg/ml in PBS buffer were incubated for ~1 hour within the flow cell, following passivation for ~2 hours of 10 mg/ml BSA (New England Biolabs). After removing non-adhered BSA by washing the flow cell with PBS, 1 pM DNA in PBS was incubated for 30 minutes at room temperature and washed out with PBS. The subsequent addition of 100 µL streptavidin-coated superparamagnetic beads (diluted 1:100 in PBS buffer; MyOne #65601 Dynabeads, Invitrogen/Life Technologies) with a diameter of 1 µm resulted in the attachment of the beads to the biotinylated end of the DNA. Prior to conducting the condensin-mediated loop extrusion experiments, the DNA tethers were assessed by applying a high force (8 pN) and 30 rotations to each direction. Only DNA tethers with singly bound DNA and correct DNA end-to-end lengths were used for the subsequent single-molecule experiments.

Since previous studies have shown that high-salt wash after ATP hydrolysis of condensin does not affect their binding to DNA for up to 1 hour (Eeftens et al., 2017), DNA tethers were re-used for multiple flush-ins of fresh constituents. Condensin was added to the flow cell in reaction buffer (20 mM Tris pH 7.5, 50 mM NaCl, 2.5 mM $MgCl_2$, 1 mM DTT, 40 µg/µL BSA) at a concentration of 1 nM or 10 nM (indicated in manuscript text) while applying 8 pN to the DNA tethers. Afterwards, the force was lowered to 0.4 pN to verify condensin binding and DNA loop-extrusion activity for 90 seconds before the attached bead was able to reach the surface, and the again to 8 pN. To wash unbound condensin out, the flow cells were washed with 500 µl reaction buffer containing 500 mM NaCl and incubated for 5 minutes. After additional washing with 300 µl of reaction buffer, ATP was injected to re-initiate DNA loop extrusion and the force was instantly (within ~1 s) adjusted to the force of interest (0.2, 0.3, 0.4, 0.5, 0.7, 1.0, 2.0, 3.0, 4.0, and 5.0 pN).

After a 5 minute observation time, the force was instantly brought back to 8 pN, accompanied by magnetic bead rotation of 20 times in each direction, to induce full DNA length recovery and rendering the DNA tethers ready for another experiment round. The same process was repeated for various forces,

and care was taken to keep the total measuring time within the time condensin stayed active (typically, <40 min).

Data analysis

The single-molecule data was processed with IGOR Pro, as previously described (Janissen et al., 2018), and further analyzed by custom-written MATLAB scripts. From our raw data, we first removed traces showing surface-adhered magnetic beads and apparent short DNA tethers where the DNA-bead attachment points were far from the 'south pole' of the beads. To do this, the method described in (Klaue and Seidel, 2009) was used. Tethers that detached from the surface during the measurement were also rejected from further analysis.

All traces resulting from experiments conducted at identical conditions were pooled by concatenating the traces together into a single time-dependent series. Prior to the step-detection analysis, all traces were filtered using a sliding median average filter over 10 data points to reduce the effect of Brownian noise. An automated step detection algorithm, described in (Kerssemakers et al., 2006), was then applied to the pooled traces for non-biased step detection. Trajectories of condensin-mediated activities were classified according to their behavior, such as loop extrusion steps consisting of consecutive downward steps, single downward steps, and single reverse steps (see examples shown in Fig. 4F). The changes in measured bead z-positions for all trajectories were converted to base pairs using base pair length values resulting from prior measured relation between the DNA end-to-end length and the applied force (Fig. S2).

Step validation and detection limit experiments

All step validation experiments were performed with PBS buffer, supplemented with 40 µg/mL BSA. Otherwise, tethered beads were prepared in identical fashion as the experiments involving condensin. Prior to the experiments, a tether test was performed to evaluate the quality of DNA tethers by applying a high force and rotations. Only tethers with singly bound DNA, correct end-to-end lengths, and non-surface adhered magnetic beads were used for the step detection experiments.

In the step validation experiments, the magnetic force was set to a fixed low value (ranging from 0.2 pN to 5 pN). Then, the piezo holding the objective was set to step up or down every 10 seconds, in multiples of 10 nm. Each sequence contained steps from 50 nm down to 10 nm, in multiples of 10 nm. Because the piezo stepping changes the position of the focal plane relative to the bead, each bead exhibited an apparent motion in multiples of 8.4 nm; a difference that stems from the change in refractive

index from immersion oil/glass to water. Depending on the pulling force, these steps were more or less submerged within the Brownian motion of the beads. After tracking the thermal fluctuations of the beads, a drift correction was applied by using the average of traces of the reference beads subtracted with the known piezo steps. Next, traces were filtered to 2 Hz with a moving median filter and subjected to step analysis (Kerssemakers et al., 2006). The parameters of the step finding algorithm were kept constant for all stepping experiments. From the step analyses, we obtained a collection of detected steps, each determined by a time of occurrence and a detected step size. This dataset was then compared with the known steps from the piezo motion. A step detection was judged correct if there was a piezo step nearby within 10% (~1s) of the expected dwell time and 30% of the expected step size. Per step size, an average success-of-detection percentage was determined over all traces. Analogously, the reverse was checked as well: a piezo step was deemed 'found' if it was seen back in the detected data using the same margins. We found that both types of detection evaluation yielded equal success percentages, as it should be expected for well-tuned step detection. We used the average of these two to obtain for each force a success percentage as a function of step size. The step size where this success percentage crossed 50% was then taken as the detection limit for each force.

FIGURES

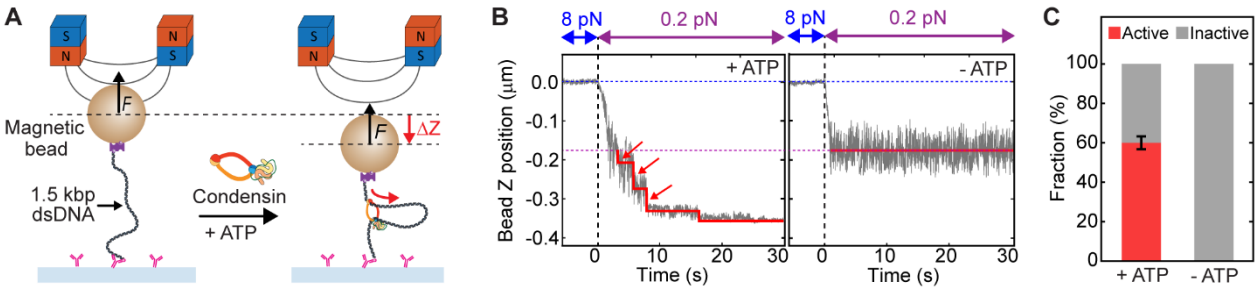

Figure 1. Step-wise DNA loop extrusion by a single condensin holocomplex. (A) Schematic of the experimental magnetic tweezers assay to monitor DNA loop extrusion by single condensins. The dotted lines showed the positions of before and upon DNA loop extrusion. **(B)** Representative trajectories of active condensin showing step-wise DNA loop extrusion in the presence of ATP (left), and inactive condensin in absence of ATP (right), at 0.2 pN DNA stretching force. Blue dotted line depicts the DNA tether length at 8 pN, and the magenta dotted line the length of bare DNA at 0.2 pN. Arrows indicate steps in the trace. Red lines are fitted steps from the step-finding algorithm. **(C)** Relative occurrence of active and inactive traces in the presence and absence of ATP for 1 nM condensin (N = 207 and 91, respectively)**.** Inactive trajectories represent either bare DNA where no condensin was bound (due to the low concentrations of condensin employed), or DNA where a condensin complex bound but could not perform loop extrusion, e.g., due to the absence of ATP.

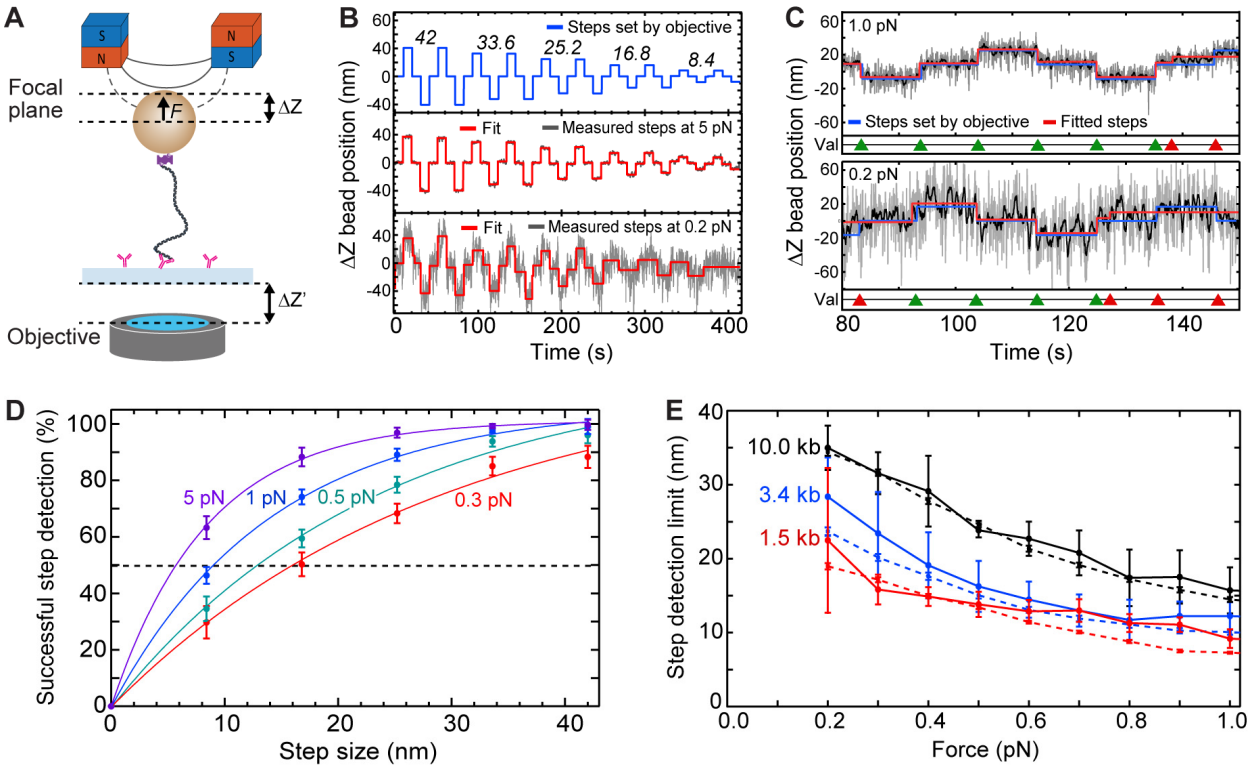

Figure 2. Step validation and step-detection limits for different DNA lengths and stretching forces. (A) Schematic for inducing changes in apparent bead Z position by changing the focal plane distance (*ΔZ*) relative to the bead. To do so, the distance between objective and sample surface (*ΔZ'*= 10, 20, 30, 40, 50 nm) was changed, which in turn changed the focal-plane distance relative to the tethered bead (*ΔZ* = 8.4, 16.8, 25.2, 33.6, 42.0 nm, respectively, accounting for the refractive index mismatch). **(B)** Example trajectories of induced *ΔZ* steps (top; *ΔZ* values in nm depicted above the corresponding induced steps), and corresponding measured bead *ΔZ* positions of a 1.5 kbp DNA at a high (5 pN; center) and low (0.2 pN; bottom) force. *ΔZ* bead position trajectories were fitted (red) with a step-finding algorithm. **(C)** Zooms of trajectories described in (B) at 1 pN (top) and 0.2 pN (bottom) DNA stretching forces. *ΔZ* bead position trajectories (grey) were filtered (black) to 2 Hz using a moving median filter, prior to applying the step-finding algorithm (red). The induced changes in *ΔZ* position (*ΔZ*=16.8 nm in the shown example) are superimposed (blue). The step-finding algorithm resulted in successful (green triangles) or unsuccessful (red triangles) detection of induced steps. **(D)** Probabilities for successful step detection (mean ± SD) versus step size for 1.5 kbp DNA at different applied DNA stretching forces. The step-detection resolution is defined as the step size where steps are successfully detected with a 50% probability (dashed line). **(E)** Step detection resolution limit versus DNA stretching force for different DNA lengths (1.5, 3.4, 10.0 kbp DNA; *N* >80 molecules for each data point). The transverse *ΔZ* bead fluctuations $\langle\sigma_z\rangle$ (dashed lines) resulting from bead Brownian motion are plotted as well. See also Fig. S2

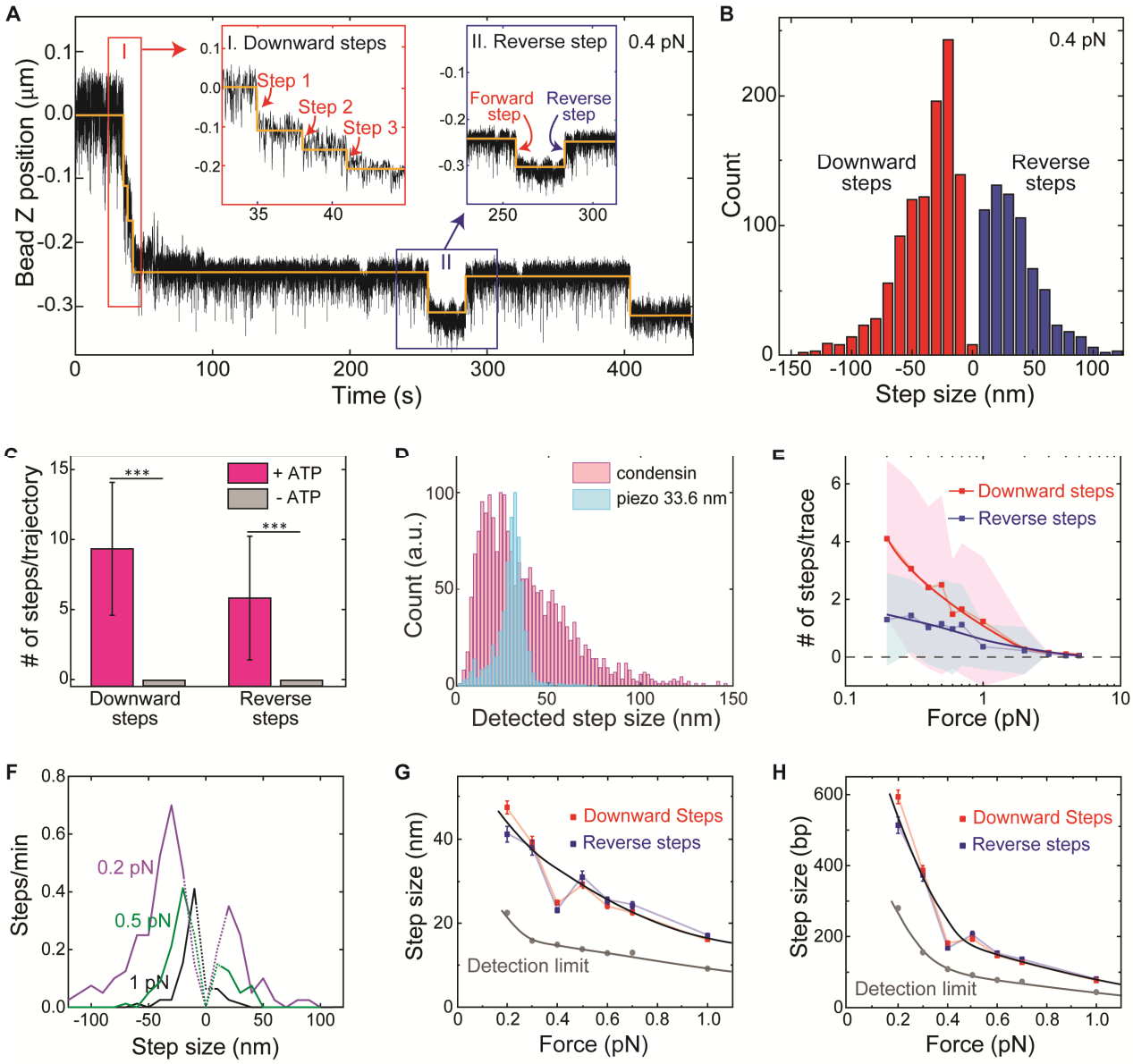

Figure 3. Broad range of force-dependent step sizes of condensin-mediated DNA loop extrusion. (**A**) Representative DNA loop-extrusion trajectory measured at 0.4 pN. Orange lines are fits of the step-finding algorithm. Insets show zooms with consecutive forward steps (left inset) and single forward and reverse steps (right). (**B**) Step size distribution for the 0.4 pN data (N = 1,727). Negative step values denote forward steps while positive values are reverse steps. (**C**) Observed number of forward and reverse steps per trajectory of 15 min in the presence and absence of ATP at 0.4 pN. Statistical analysis consisted of an unpaired two-tailed t-test (*** indicates $p < 0.001$). (**D**) Step size distributions of condensin-mediated DNA loop extrusion (magenta, N = 5,128) and piezo-induced artificial step size of 33 nm (cyan, N = 1,069) at 0.4 pN. (**E**) Average number of forward and reverse steps (mean ± SD) per 2-minute trace (N = 108, 90, 67, 73, 48, 57, 31, 23, 11, 6, 4 from 0.2 to 5.0 pN). (**F**) Step size distributions for different DNA stretching forces.

Dotted lines denote the range below the step detection limit. Data for other forces are provided in SI. (**G**) Forward (N > 500 for each force) and reverse step (N > 300 for each force) sizes in nm (median ± SEM) verse force. (**H**) Same as G but step size in now given in base pairs. Step size in base pair was calculated using the measured relation between the DNA end-to-end length and the applied force. The detection limit in G and H was obtained from Fig. 2E. See also Figs. S3 and S4.

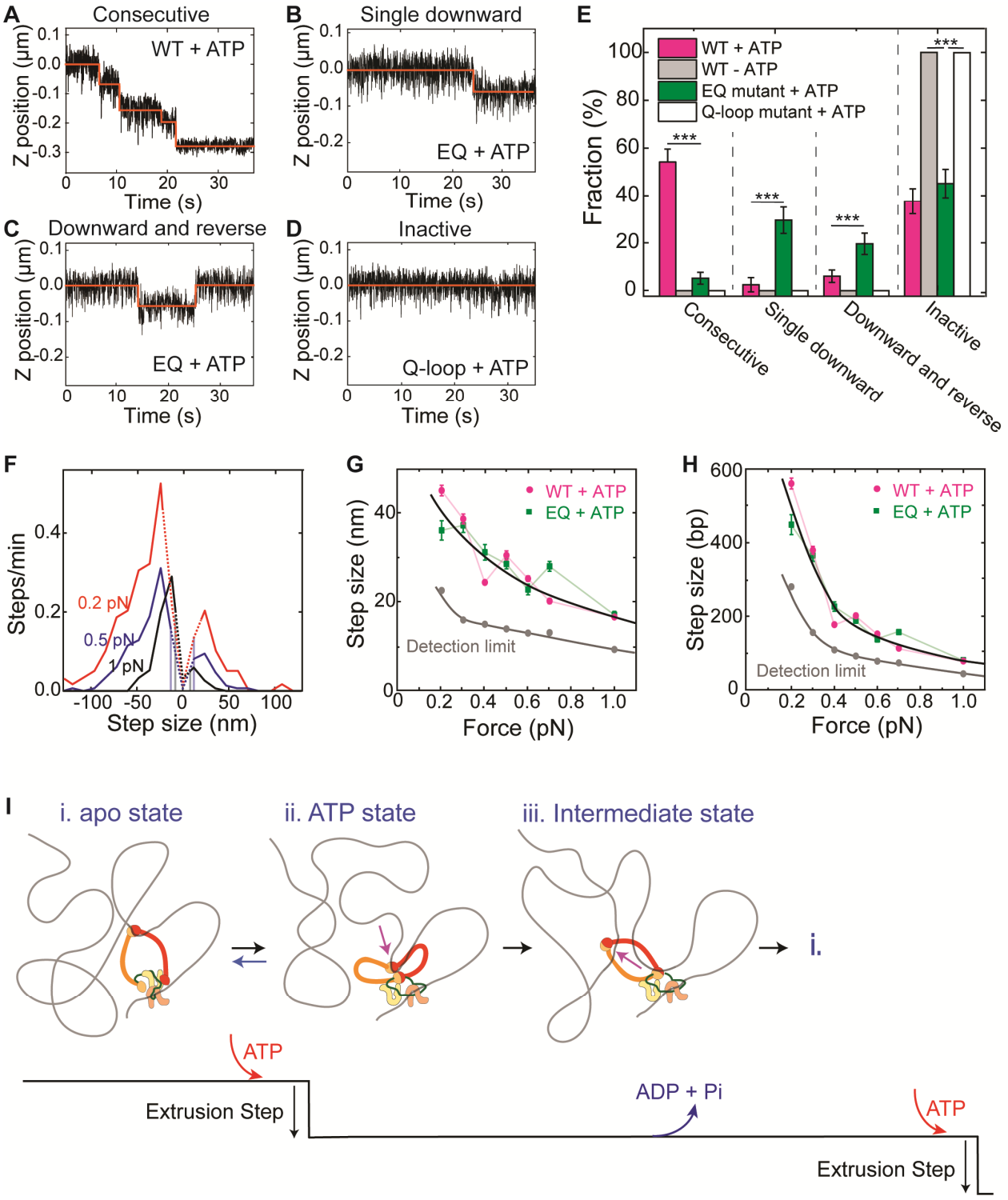

Figure 4. ATP-binding of condensin induces a single step in DNA loop extrusion. (A-D) Representative trajectories for (A) consecutive DNA loop extrusion steps, (B) a single forward step, (C) a single forward followed by a reverse step, and (D) an inactive trajectory, all probed in the presence of ATP. **(E)** Observed fractions of different stepping behavior (*N* = 85, 96, 77, and 18 for wild-type with ATP, without ATP, EQ

mutant with ATP, and Q-loop mutant with ATP, respectively). Statistical analysis consisted of an unpaired two-tailed t-test (*** indicates $p < 0.001$). **(F)** Step size distributions of the EQ mutant in the presence of ATP at different DNA stretching forces (median ± SD; 0.2 pN: N = 154; 0.5 pN: N=186; 1 pN: N=106). Dotted lines denote step sizes below the step resolution limit. Data for other forces are provided in SI. **(G)** Step size in nm (median ± SEM) for WT (magenta) and EQ mutant (green) versus applied force (0.2 pN: N = 69; 0.3 pN: N = 53; 0.4 pN: N = 73; 0.5 pN: N = 74; 0.6 pN: N = 45; 0.7 pN: N = 58; 1 pN: N = 76). Forward and reverse steps were pooled together in these data. (**H**) Same as G but converted to step size in base pairs. The detection limit in G and H was obtained from Fig. 2E. **(I)** Proposed working model for the condensin conformational changes during the ATP hydrolysis cycle. (i) Condensin holocomplex is anchored to DNA by the Ycg1-Brn1 subunit. In the open configuration, the hinge domain binds DNA. Note that the hinge grabs an arbitrary nearby location within the randomly structured DNA polymer coil. (ii) Upon ATP binding to condensin, the SMC ring changes from the open to a collapsed (butterfly) configuration, generating a single DNA loop-extrusion step where DNA is reeled in via the hinge movement. From our data, we conclude that this step is in principle reversible, whereby state *ii* can return to state *i*. (iii) After DNA transfer to the globular domain of condensin, the hinge is released, presumably during ATP hydrolysis, whereupon it is available to bind new DNA for the next step in the cycle. Upon repetition of this cycle, DNA is extruded into an expanding loop in consecutive steps. See also Fig. S4.

SUPPLEMENTAL INFORMATION

Table S1: Primer sequences used for the synthesis of linear DNA tether constructs.

Oligonucleotide	Sequence
JT-273	5'-Biotin-GCAATAAACCAGCCAGCCGGAAG
JT-275	5'-TTTTTTTTTTGGTCTCTATACTACCGTCGACCTCGAGGG
CD-21	5’-GACCGAGATAGGGTTGAGTG
CD-26	5’-TTTTTTTTTTGGTCTCTGTATCTGGCGTTACCCAACTTAATCGCC
TL-34	5'-Biotin-GACCGAGATAGGGTTGAGTG
TL-35	5’-CAGGGTCGGAACAGGAGAG
TL-101	5'-Biotin- CTGCGGTCTCGTAGGCCGATTTAGAGCTTGACGGGG
TL-102	5’- CTGCGGTCTCGCGGGTTGCAGCACTGGGGCCAGATG

SUPPLEMENTARY FIGURES

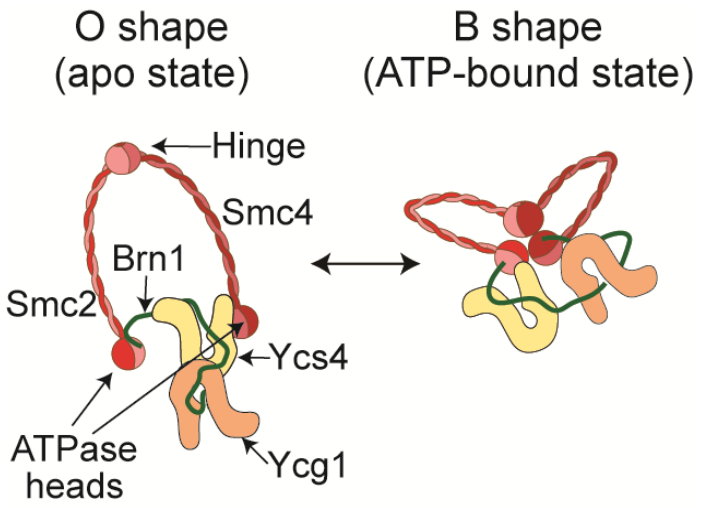

Figure S1. Structural domains of the yeast condensin holocomplex. The condensin holocomplex consists of two antiparallel folded coiled-coil arms, Smc2 and Smc4 (each ~50 nm in length), mutually linked to a hinge domain dimer at one end, and an ATP-binding cassette (ABC)-type nucleotide-binding head domain at the other end, where the two head domains are mutually connected by the Brn1 kleisin subunit. Two HEAT-repeat subunits, Ycs4 and Ycg1, are bound to the Brn1 kleisin subunit. Recent AFM data (Ryu et al., 2020) indicated an O-shape apo state, where the hinge is located far from the globular domain, and a B shape ATP-bound state where the hinge is in close proximity of the globular domain.

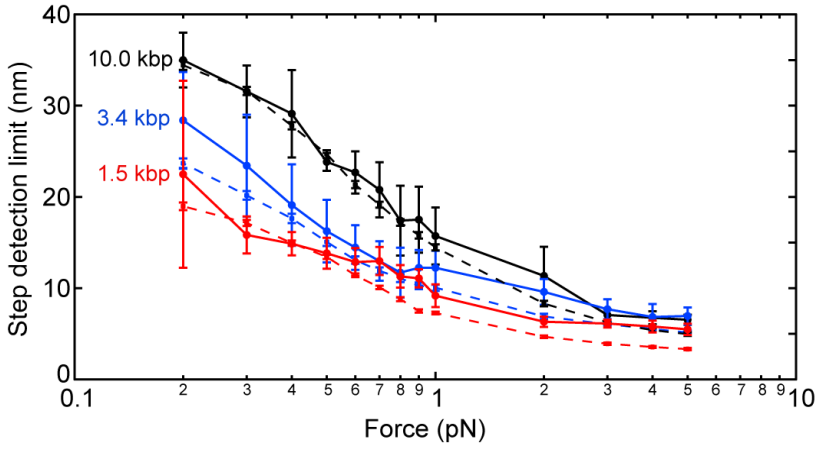

Figure S2. Step-detection limits for different DNA lengths and stretching forces. Step detection resolution limit versus DNA stretching force (0.2 – 5 pN) for different DNA lengths (1.5, 3.4, 10.0 kbp DNA; N >80 molecules for each data point). The transverse ΔZ bead fluctuations $\langle\sigma_z\rangle$ (dashed lines) resulting from bead Brownian motion are plotted as well. Related to Fig. 2.

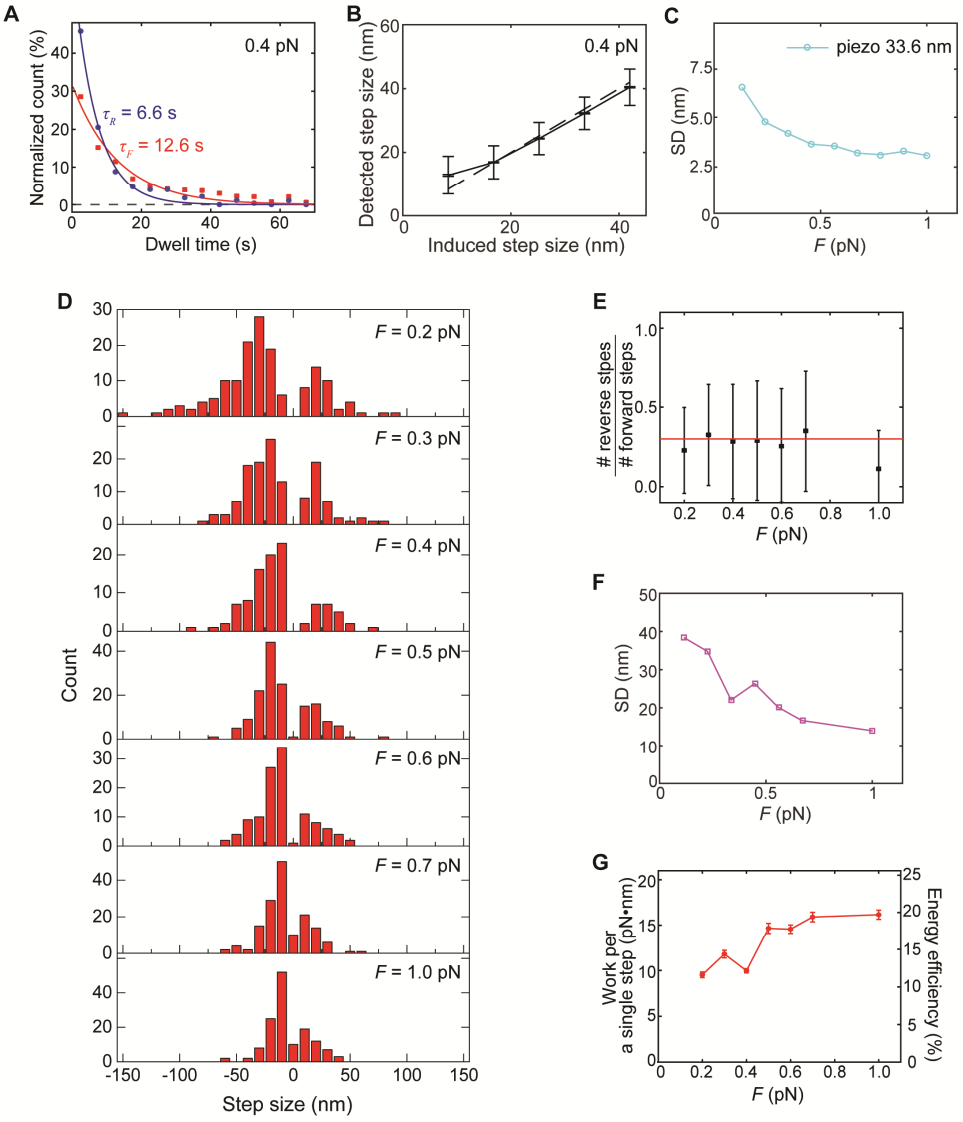

Figure S3. Characterization of piezo-induced and condensin-mediated DNA- extrusion steps at different forces. (**A**) Dwell-time distributions of downward (red; *N* = 273) and reverse steps (blue; *N* = 665) that show single-exponential fits (solid lines) with time constants τ_F and τ_R, respectively. (**B**) Detected step sizes versus induced step sizes for the different piezo-induced step sizes at 0.4 pN (median ± SD). *N* = 255, 870, 1033, 1069, and 1063 for 8.4, 16.8, 25.2, 33.6, and 42 nm step sizes, respectively. **(C)** Force-dependent width (SD) as function of applied force, for the detected step size distributions from piezo-induced artificial step sizes of 33.6 nm (*N* = 994, 1060, 1069, 989, 987, 942, 1,000, 852, and 847 for 0.2, 0.3, 0.4, 0.5, 0.6, 0.7, 0.8, 0.9, and 1 pN, respectively). (**D**) The ratio between number of reverse steps and downward steps observed at different DNA stretching forces (mean ± SD; *N* > 500 for each force). Red line depicts the average of the data (y = 0.3). **(E)** Step size distributions with different forces (*N* = 153, 131, 102, 154, 118, 155 and 140 for 0.2, 0.3, 0.4, 0.5, 0.6, 0.7, 0.8, 0.9, and 1 pN, respectively**) (F)** Width (SD) of detected step size distributions versus applied force for condensin-induced step (*N* > 500). (**G**) The work done ($F \times step\ size$) in each single DNA extrusion step, plotted versus force (median ± SEM; *N* > 500 for each force). Right axis denotes the corresponding energy efficiency (%). Related to Fig. 3.

A

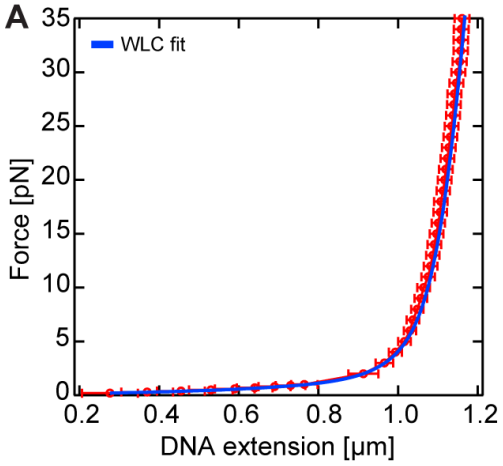

B

Force (pN)	L_{bp} (nm)	Force (pN)	L_{bp} (nm)
8	0.3078	0.9	0.1986
7	0.3039	0.8	0.1898
6	0.2992	0.7	0.1780
5	0.2933	0.6	0.1657
4	0.2853	0.5	0.1509
3	0.2737	0.4	0.1373
2	0.2545	0.3	0.1017
1	0.2115	0.2	0.0802

Figure S4. Conversion from nanometers to base pairs at different forces. (**A**) Force-extension data of linear 3.4 kbp dsDNA (red; mean ± SD; N = 32), fitted to a WLC model, providing a persistence length L_P = 42 nm, and contour length L_C = 1.16 µm. (**B**) dsDNA base pair length (L_{bp}) in nanometer extracted from the WLC fit in (A) for the different forces applied in the condensin experiments. Related to Figs. 3 and 4.